Electronic Supplementary Material (ESI) for Journal of Materials Chemistry A.

Transparent and colour-neutral luminescent solar concentrators using bright Eu^{3+} supramolecular cages towards photovoltaic windows

Irene Motta,[a] Gregorio Bottaro,[*b] Maria Rando,[a] Marzio Rancan,[*b] Roberta Seraglia,[c] Lidia Armelao[a,d]

[a]Department of Chemical Sciences (DiSC), University of Padova, via F. Marzolo 1, 35131 Padova, Italy;

[b]Institute of Condensed Matter Chemistry and Technologies for Energy (ICMATE), National Research Council (CNR), c/o Department of Chemical Sciences (DiSC), University of Padova, via F. Marzolo 1, 35131 Padova, and National Interuniversity Consortium of Materials Science and Technology (INSTM), Florence, Italy,

[c]Institute of Condensed Matter Chemistry and Technologies for Energy (ICMATE), National Research Council (CNR), Corso Stati Uniti 4, Corso Stati Uniti, 4, 35127 Padova PD

[d]Department of Chemical Sciences and Materials Technologies (DSCTM), National Research Council (CNR), Piazzale A. Moro 7, 00185 Roma, Italy; and National Interuniversity Consortium of Materials Science and Technology (INSTM), Florence, Italy,

Supplementary Information

Synthetic procedures

All chemicals were purchased from Merck and used as received. The bis-β-diketone ligands L^B, L^M and L^A and pre-L^A, as well as the $[Eu_2L_4]^{2-}$ cages, were prepared according to previous reports[1,2]. $Eu(tta)_3phen$ was synthesized according to literature[3].

$Eu(tta)_3phen$: 2-thenoyltrifluoroacetone (1.72 g, 7.7 mmol) and 1,10-phenathroline (0.46 g, 2.6 mmol) have been dissolved in 40 mL of ethanol at 60 °C. An ethanolic solution of NaOH (50 mL) has been added to the above solution. $EuCl_3 \cdot 6H_2O$ (0.96 g, 2.6 mmol) in ethanol (70 mL) has been added dropwise, observing immediate formation of a white precipitate. After reacting for 4 hours, the mixture has been left at 0°C overnight. The precipitate has been filtered, dried over $CaCl_2$ under vacuum and purified by hot filtration from THF at 50°C. The final product has been obtained as a yellowish white powder (1.96 g). Yield: 75%.

L^F: Metallic Na (≈1 g, 43.5 mmol) has been dissolved in 40 mL of ethanol under Ar atmosphere. Ethyl trifluoroacetate (5.0 mL, 42.0 mmol) has been added together with pre-L (≈6 mmol). Ethyl pentafluoropropionate (6.2 mL, 42.0 mmol) has been added has been added together with pre-L (≈ 6 mmol) pre-L^A. After stirring at room temperature overnight, the solvent has been removed under reduced pressure. Water (100 mL) and an HCl 10% aqueous solution (15 mL) have been added, observing the formation of a precipitate. The solution has been extracted with CH_2Cl_2 (3x60 mL), the organic phase has been dried over $MgSO_4$ and the solvent has been removed under reduced pressure, resulting in a dark orange oil.. The product has been purified by recrystallization (acetonitrile/water 1:4). Yields: 72 %.

$\{[Eu_2L_4](NEt_4)_2\}$: The ligand (0.05 mmol) and the base (tetraethylammonium hydroxide, (0.1 mmol) have been dissolved in 2 mL of ethanol. A a solution of $EuCl_3 \cdot 6H_2O$ (0.020 mmol) in 1 mL of ethanol has been added dropwise, observing immediate formation of a white precipitate. The ratio Eu^{3+}:ligand:base used was 1:2.5:5. After stirring for 3 hours at 50°C, the solution has been centrifugated with cold ethanol (3x5mL) and the solid dried on $CaCl_2$ under vacuum to give the pure product. Yields: 30 %.

Single Crystal X-ray diffraction

Single crystals for the Eu cage were obtained from mother liquors (ethanol) after two weeks. Ligand L^F single crystal were obtained by slow evaporation of an acetonitrile/water (1:4) solution.

Data for ligand L^F were collected using an Oxford Diffraction Gemini E diffractometer, equipped with a 2K × 2K EOS CCD area detector and sealed–tube Enhance (Mo) and (Cu) X–ray sources. A suitable single crystal of L^F was fastened on a nylon loop and measured at room temperature. Empirical multi-scan absorption corrections using equivalent reflections have been performed with the scaling algorithm SCALE3 ABSPACK. Data reduction, finalization and cell refinement were carried out through the CrysAlisPro software. Accurate unit cell parameters were obtained by least squares refinement of the angular settings of strongest reflections, chosen from the whole experiment.

A suitable crystal for the Eu cage was mounted at room temperature in NVH oil and measured at 150K. Data were collected on a Bruker D8 Venture diffractometer equipped with Incoatec IμS3.0 (EF) microfocus sealed-tube (Cu-Kα, λ = 1.54178 Å), a Montel layer optics monochromator, and a Photon III C14 CPAD area detector. Data integration was done with SAINT, data scaling and absorption correction were performed with SADABS, in the APEX3 software.

The structures were solved with Olex2[4] by using ShelXT[5] structure solution program by Intrinsic Phasing and refined with the ShelXL[6] refinement package using least-squares minimization. In the last cycles of refinement, non-hydrogen atoms were refined anisotropically. Hydrogen atoms were included in calculated positions, and a riding model was used for their refinement. Details for Eu cage structure refinement are reported below along with crystallographic table (Table S1) and asymmetric unit images.

Cambridge Crystallographic Data Centre (CCDC) numbers 2349361 and 2349362 contain the supplementary crystallographic data for this paper. These data are provided free of charge by the joint CCDC and Fachinformationszentrum Karlsruhe Access Structures service www.ccdc.cam.ac.uk/structures.

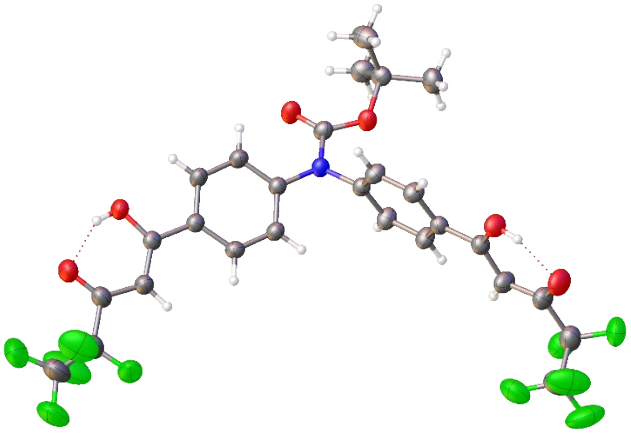

Figure S1. The asymmetric unit of L^F, thermal ellipsoid drawn at 30% probability level. Color code: C, grey; O, red; N, blue; F, green; H, white.

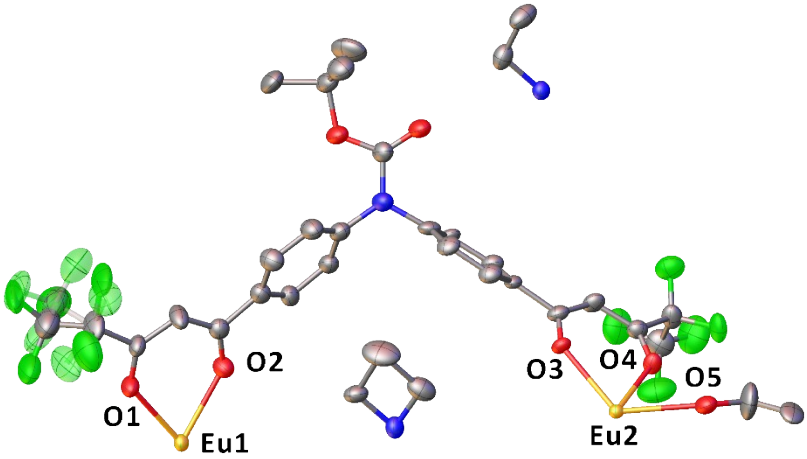

Figure S2. The asymmetric unit for {[$Eu_2L^F_4$])(NEt_4)$_2$} cage, thermal ellipsoid drawn at 50% probability level. Color code: C, grey; O, red; N, blue; F, green; Eu, orange. Disordered parts translucent. H atoms omitted for clarity.

Refinement details for Eu cage

The compound crystallizes in the *P*4/*ncc* space group. In the asymmetric unit, a quarter of the cage is present. One of the two terminal fluorinated groups has been split in two parts the occupancies of which were constrained to sum to 1.0. Ligand and ethanol molecule were modelled with the help of the FragmentDB plugin[7] in the framework of OLEX2. RIGU restraints were applied. The final Fourier map revealed the presence of non-negligible residual peaks located in a large array of voids. A total accessible void volume per unit cell of 1772 Å^3 was calculated (SQUEEZE,[8] probe radius 1.2 Å) corresponding to the 11.9% of the total unit cell volume divided in four voids of 443 Å^3 each. A single void contains 103 electrons. This value closely close fits the presence of 4 ethanol molecules accounting for 96 electrons.

Table S1 Crystal data and structure refinement.

	L^F	**{[$Eu_2L^F_4$])(NEt_4)$_2$}**
Empirical formula	$C_{27}H_{21}F_{10}NO_6$	$C_{126}H_{122}Eu_2F_{40}N_6O_{25}$
Formula weight/ g mol^{-1}	645.45	3184.21
Temperature/K	297.1(3)	150.00
Crystal system	triclinic	tetragonal
Space group	P-1	P4/ncc
a/Å	5.66571(15)	18.6338(5)
b/Å	14.1061(4)	18.6338(5)
c/Å	18.5822(6)	42.6165(19)
α/°	72.299(3)	90
β/°	85.374(2)	90
γ/°	88.917(2)	90
Volume/Å^3	1410.17(7)	14797.2(10)
Z	2	4
ρ_{calc} / g cm^3	1.520	1.429
μ/mm^{-1}	1.336	7.027

F(000)	656.0	6424.0
Crystal size/mm^3	0.15 × 0.21 × 0.22	0.089 × 0.082 × 0.041
Radiation	Cu Kα (λ = 1.54184)	CuKα (λ = 1.54178)
2Θ range for data collection/°	6.954 to 140.924	4.146 to 148.972
Index ranges	-5 ≤ h ≤ 6, -17 ≤ k ≤ 17, -22 ≤ l ≤ 20	-22 ≤ h ≤ 23, -23 ≤ k ≤ 21, -53 ≤ l ≤ 53
Reflections collected	14833	166245
Independent reflections	5259 [Rint = 0.0319, Rsigma = 0.0303]	7570 [Rint = 0.1300, Rsigma = 0.0394]
Data/restraints/parameters	5259/0/402	7570/710/531
Goodness-of-fit on F^2	1.048	1.024
Final R indexes [I>=2σ (I)]	R1 = 0.0710, wR2 = 0.2043	R1 = 0.0896, wR2 = 0.2404
Final R indexes [all data]	R1 = 0.0976, wR2 = 0.2345	R1 = 0.1120, wR2 = 0.2609
Largest diff. peak/hole / e Å^{-3}	0.41/-0.29	1.71/-1.82
CCDC number	2349361	2349362

Continuous shape measures analysis

A continuous shape measures analysis of Eu ions coordination polyhedra has been performed with the SHAPE 2.1 software considering an eight-coordination for Eu1 and a nine-coordination for Eu2. The closer the value to zero, the better it fits to the ideal geometry.

Table S2. Coordination geometries evaluated for the eight-coordination of Eu1 and output of the SHAPE 2.1 software for Eu1.

Abbreviation	Ideal geometry	Symmetry	Output
OP-8	Octagon	D_{8h}	27.195
HPY-8	Heptagonal pyramid	C_{7v}	24.486
HBPY-8	Hexagonal bipyramid	D_{6h}	15.677
CU-8	Cube	O_h	7.954
SAPR-8	**Square antiprism**	$\boldsymbol{D_{4d}}$	**0.334**
TDD-8	Triangular dodecahedron	D_{2d}	2.275
JGBF-8	Johnson gyrobifastigium J26	D_{2d}	16.227
JETBPY-8	Johnson elongated triangular bipyramid J14	D_{3h}	28.892
JBTPR-8	Biaugmented trigonal prism J50	C_{2v}	2.992
BTPR-8	Biaugmented trigonal prism	C_{2v}	2.188
JSD-8	Snub disphenoid	D_{2d}	5.412
TT-8	Triakis tetrahedron	T_d	8.831
ETBPY-8	Elongated trigonal bipyramid	D_{3h}	23.763

Table S3. Coordination geometries evaluated for the eight-coordination of Eu1 and output of the SHAPE 2.1 software for Eu2.

Abbreviation	Ideal geometry	Symmetry	Output
EP-9	Enneagon	D_{9h}	38.385
OPY-9	Octagonal pyramid	C_{8v}	20.890
HBPY-9	Heptagonal bipyramid	D_{7h}	21.309
JTC-9	Triangular cupola (J3) = trivacant cuboctahedron	C_{3v}	17.511
JCCU-9	Capped cube (Elongated square pyramid, J8)	C_{4v}	10.960
CCU-9	Capped cube	C_{4v}	9.774
JCSAPR-9	Capped sq. antiprism (Gyrœlongated square pyramid J 10)	C_{4v}	1.025
CSAPR-9	**Capped square antiprism**	$\boldsymbol{C_{4v}}$	**0.029**
JTCTPR-9	Tricapped trigonal prism (J51)	D_{3h}	2.849
TCTPR-9	Tricapped trigonal prism	D_{3h}	1.116
JTDIC-9	Tridiminished icosahedron (J63)	C_{3v}	13.660
HH-9	Hula-hoop	C_{2v}	13.549
MFF-9	Muffin	C_S	0.897

Electrospray mass spectrometry (ESI-MS)

Electrospray mass spectrometric measurements (ESI-MS) were performed using a LCQ Fleet ion trap instrument (ThermoFisher), equipped with a HESI source, operating in negative ion mode. The mass spectra were acquired using the following experimental parameters: T_{HESI} = 35 °C; $T_{transfer\ capillary}$= 275 °C; Voltage HESI= 4 kV; nebulizer gas flow rate (N_2): 10 a.u.; auxiliary gas flow rate (N_2): 5 a.u. Sample solutions (10^{-6} M in acetonitrile) were introduced by direct infusion using a syringe pump at a flow rate of 8 μl·min^{-1}.

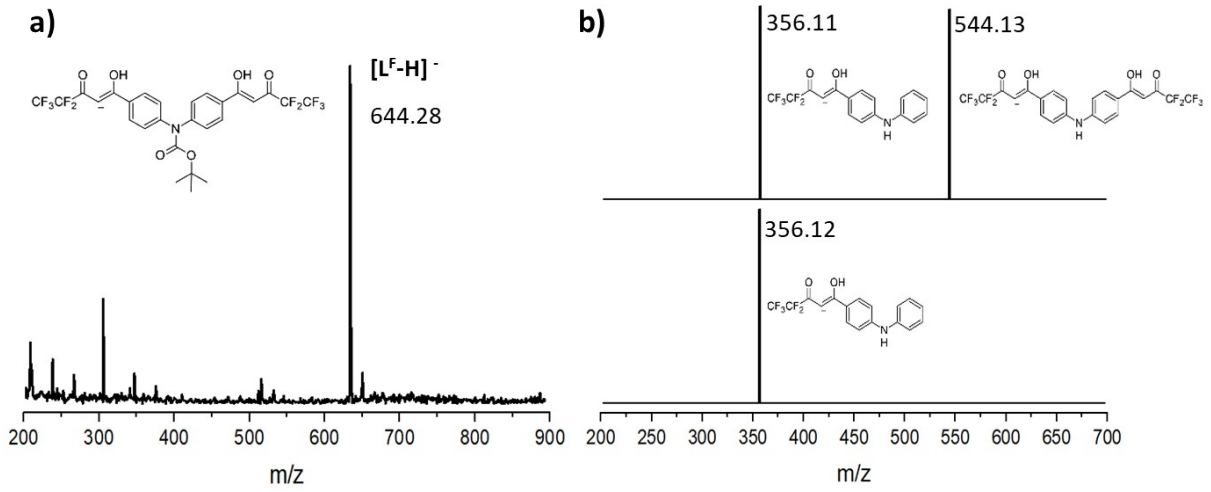

Figure S3. **a)** ESI-MS spectrum of the L^F ligand. **b)** MS/MS fragmentations relative to 644.28 m/z (top) and 544.13 m/z signals (bottom).

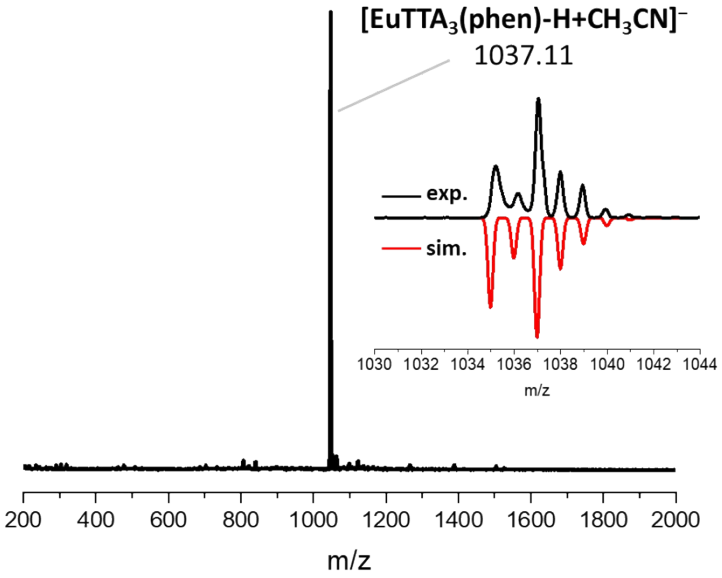

Figure S4. Electrospray mass spectra of [Eu(tta)$_3$phen]. Inset: experimental (black line) and simulated (red line) isotopic pattern.

Table S4. Labelling of the prepared LSCs and of the corresponding devices obtained by edge-coupling monocrystalline Si solar cell to the LSCs.

LSC	Device	Luminophore	Concentration / wt %
LSC-A	**LSC-A^{PV}**	$[Eu_2L^A_4]^{2-}$	0.005
LSC-F	**LSC-F^{PV}**	$[Eu_2L^F_4]^{2-}$	
LSC-B	**-**	$[Eu_2L^B_4]^{2-}$	
LSC-M	**-**	$[Eu_2L^M_4]^{2-}$	
LSC-T	**LSC-T^{PV}**	Eu(tta)$_3$phen	
LSC-Fc	**LSC-Fc^{PV}**	$[Eu_2L^F_4]^{2-}$	0.1
LSC-Tc	**LSC-Tc^{PV}**	Eu(tta)$_3$phen	0.5
PM	**PM^{PV}**	none	/

Table S5. Average visible transmittance (AVT), color rendering index (CRI), (a*, b*) CIELAB coordinates and total absorptance ($\eta_{s,abs}$) calculated for the selected LSCs.

	AVT / %	CRI	*a**	*b**	$\eta_{s,abs}$ / %
LSC-A	92.24	99.51	-0.05	0.43	0.62
LSC-F	92.27	99.53	-0.04	0.41	0.57
LSC-Fc	92.17	99.52	-0.05	0.43	1.11
LSC-T	92.35	99.64	-0.02	0.32	0.40
LSC-Tc	91.82	98.40	-0.38	1.42	1.81
PM	92.41	99.73	0.01	0.23	/

Table S6. Recommended parameters for LSC-PV characterization, adapted from reference. [9]

LSC-PV reporting recommendations.

Property	Explanation	Report
Device structure	Length, width, thickness, geometric gain (G), PV cell type, edge (PV cell, mirrors, blackened).	Recommended
Luminophore/lightguide	Absorptance, emission spectra, PLQY of luminophores.	Recommended
Power Conversion Efficiency (PCE)	Including J-V characteristics and device active area (A_{active}).	Recommended
External Quantum Efficiency ($EQE_{LSC}(\lambda)$)	Identifies measurement artifacts, includes scalability and consistency check for J_{sc}.	Recommended
Internal Photon Efficiency (η_{int})	Includes internal losses such as reabsorption, PLQY and scattering.	Recommended
External Photon Efficiency (η_{ext})	Includes all losses including reflection and transmission losses.	Optional
Average Visible Transmittance (AVT)	With colour rendering index (CRI) and CEILAB colour space (a*, b*).	Optional
Concentration Ratio (C)	Useful for LSC devices utilising high cost PV cells.	Optional

The Matlab Live Script for the calculation of recommended LSC-PV reporting parameters and a sample dataset to test the functionality of the script can be downloaded from the following link:

https://it.mathworks.com/matlabcentral/fileexchange/166426-luminescent-solar-concentrators-pv-characterization

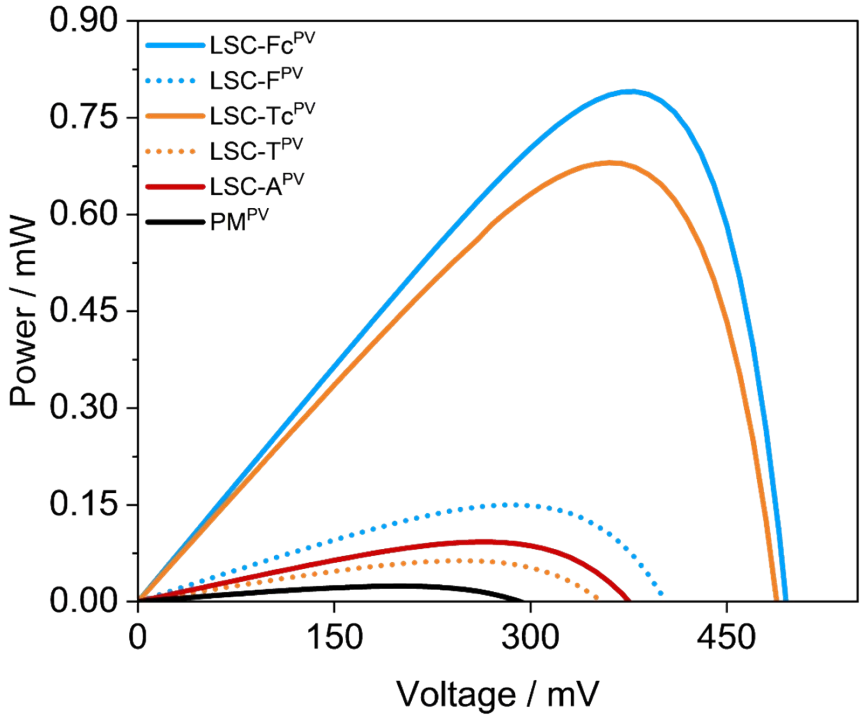

Figure S5. Power-voltage data measured for the prepared LSC-PV devices.

Table S7. Short-circuit current density (J_{SC}), open-circuit voltage (V_{OC}), fill factor (FF), maximum power (P_{MAX}) and power conversion efficiency (PCE) values of tested LSC-PVs at lower luminophore loadings.

	J_{SC} / mA/cm²	V_{OC} / mV	FF	P_{MAX} / mW	PCE / % 1 edge	*PCE / % 4 edges
LSC-A^{PV}	0.018	375	0.55	0.093	0.0037	0.0148
LSC-F^{PV}	0.026	403	0.57	0.150	0.0060	0.0240
LSC-T^{PV}	0.013	355	0.54	0.063	0.0025	0.0100
PM^{PV}	0.007	292	0.50	0.024	0.0010	0.0040

*Calculated multiplying PCE by 4

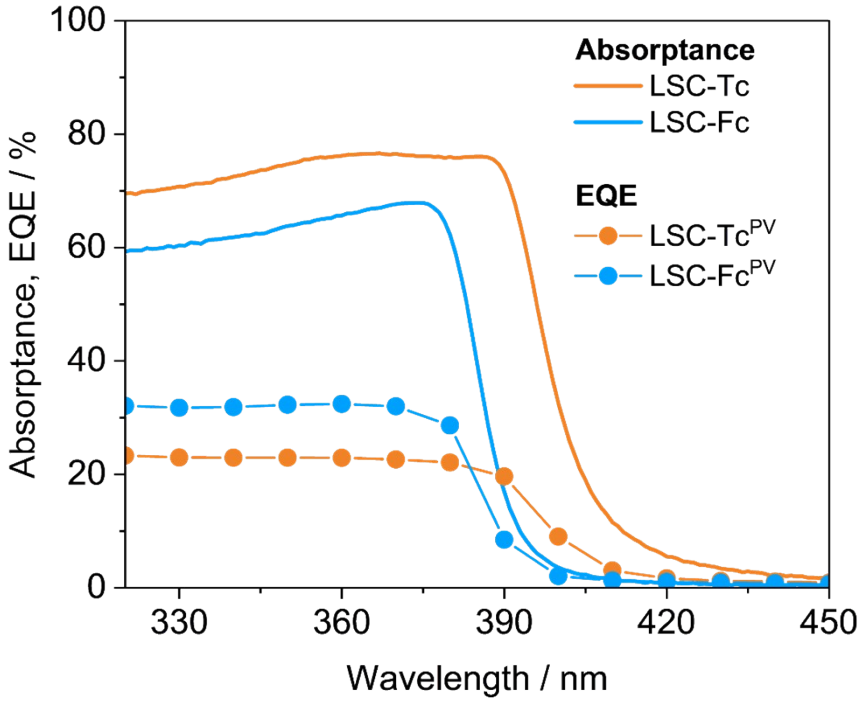

Figure S6. Absorptance spectra of **LSC-Fc** and **LSC-Tc**, and EQE spectra of the corresponding LSC-PVs. Displayed EQE spectra have been derived by applying a multiplicative correction factor of 4 to one-edge measurements.[10]

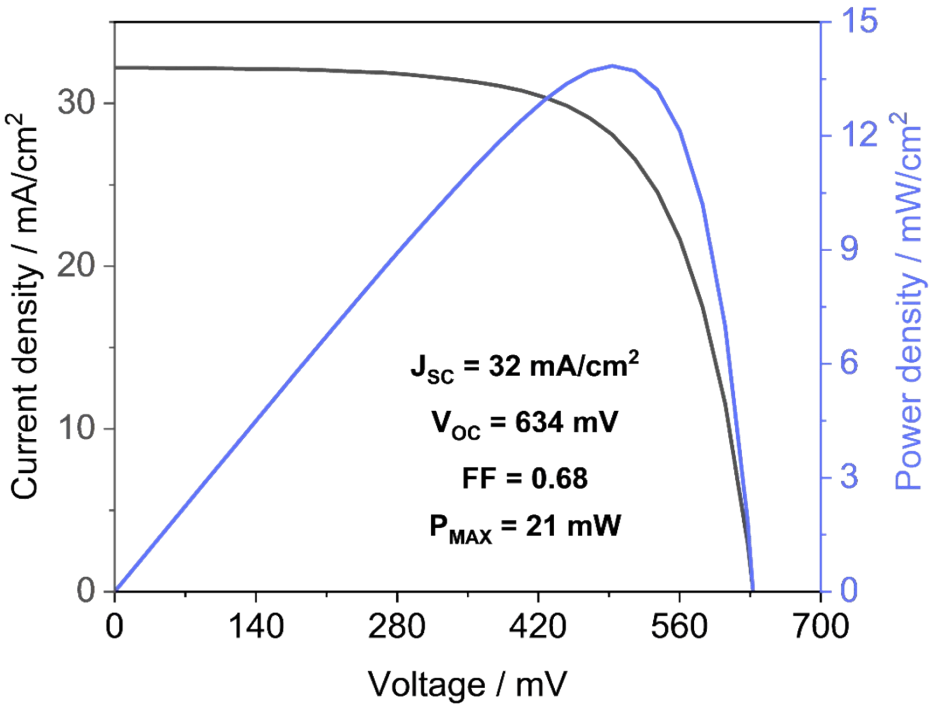

Figure S7. Illustrative measured J-V and P-V characteristics of the adopted Si PV cells, along with derived electrical parameters.

Bibliographic references

1 M. Rancan, J. Tessarolo, A. Carlotto, S. Carlotto, M. Rando, L. Barchi, E. Bolognesi, R. Seraglia, G. Bottaro, M. Casarin, G. H. Clever and L. Armelao, *Cell Reports Physical Science*, 2022, **3**, 100692.

2 M. Rancan, M. Rando, L. Bosi, A. Carlotto, R. Seraglia, J. Tessarolo, S. Carlotto, G. H. Clever and L. Armelao, *Inorg. Chem. Front.*, 2022, **9**, 4495–4505.

3 L. R. Melby, N. J. Rose, E. Abramson and J. C. Caris, *J. Am. Chem. Soc.*, 1964, **86**, 5117–5125.

4 O. V. Dolomanov, L. J. Bourhis, R. J. Gildea, J. a. K. Howard and H. Puschmann, *J Appl Cryst*, 2009, **42**, 339–341.

5 G. M. Sheldrick, *Acta Cryst A*, 2015, **71**, 3–8.

6 G. M. Sheldrick, *Acta Cryst C*, 2015, **71**, 3–8.

7 D. Kratzert and I. Krossing, *J Appl Crystallogr*, 2018, **51**, 928–934.

8 A. L. Spek, *Acta Cryst C*, 2015, **71**, 9–18.

9 T. Warner, K. P. Ghiggino and G. Rosengarten, *Solar Energy*, 2022, **246**, 119–140.

10 C. Yang, D. Liu and R. R. Lunt, *Joule*, 2019, **3**, 2871–2876.